Ken R. Duffy[1]
Neil Gurram[2]
Kelsey C. Peters[3]
Genevieve Wellner[3]
Catherine M. Grgicak[3]

[1]Hamilton Institute, Maynooth University, Maynooth, Ireland
[2]Research Laboratory of Electronics, Massachusetts Institute of Technology, Cambridge, MA, USA
[3]Biomedical Forensic Sciences, Boston University School of Medicine, Boston, MA, USA

Received August 22, 2016
Revised November 10, 2016
Accepted November 29, 2016

Research Article

Exploring STR signal in the single- and multicopy number regimes: Deductions from an in silico model of the entire DNA laboratory process

Short tandem repeat (STR) profiling from DNA samples has long been the bedrock of human identification. The laboratory process is composed of multiple procedures that include quantification, sample dilution, PCR, electrophoresis, and fragment analysis. The end product is a short tandem repeat electropherogram comprised of signal from allele, artifacts, and instrument noise. In order to optimize or alter laboratory protocols, a large number of validation samples must be created at significant expense. As a tool to support that process and to enable the exploration of complex scenarios without costly sample creation, a mechanistic stochastic model that incorporates each of the aforementioned processing features is described herein. The model allows rapid in silico simulation of electropherograms from multicontributor samples and enables detailed investigations of involved scenarios. An implementation of the model that is parameterized by extensive laboratory data is publically available. To illustrate its utility, the model was employed in order to evaluate the effects of sample dilutions, injection time, and cycle number on peak height, and the nature of stutter ratios at low template. We verify the model's findings by comparison with experimentally generated data.

Keywords:
Analytical threshold / Electropherogram signal model / Forensic DNA / Short tandem repeats / Single-copy DNA analysis DOI 10.1002/elps.201600385

1 Introduction

Since the work describing PCR was published [1], analysis of short tandem repeat (STR) fragments has been the mainstay of the forensic identity process. Once biological evidence is collected and submitted to the DNA laboratory, extraction and purification of the DNA ensue. The extract is quantified, typically using quantitative PCR (qPCR) methods and, if necessary, diluted. Next, PCR is utilized as a means to exponentially amplify the number of DNA copies from a set of STR regions. The STR loci commonly employed during human identity testing were chosen because they are relatively short in length (3–5 bp sequences that repeat 5–40 times) and are polymorphic among individuals. Once amplification is complete, STR fragment analysis is accomplished by electrophoresis where the amplicons are separated based on size and the intensity of the fluorescence signal is indicative of the number of amplicons produced during PCR [2–6].

Though STR profiling is common practice, the interpretation of STR measurements is complicated by the presence of instrument noise and PCR artifacts such as stutter. Both are difficult to distinguish from allele signal, particularly when there are only a few cells available for testing. The complexity associated with STR interpretation quickly escalates with the number of, usually unknown, contributors to the DNA mixture [7–10].

In crime laboratories, the identification of which alleles are present in the sample is typically determined by applying an analytical threshold (AT) in order to filter background noise from allele signal in the electropherogram (EPG) [11]. With the application of an AT, there are potentially three reasons an allele may not be detected: (i) the allele was not present in the amplification tube; (ii) the allele was present and was amplified, but there was insufficient starting quantity of DNA to cross the AT; or (iii) the allele was present and was amplified, but PCR replication was inefficient and the

Correspondence: Dr. Catherine M. Grgicak, Biomedical Forensic Sciences, Boston University School of Medicine, 72 East Concord Street, Room R806, Boston, MA 02118, USA
E-mail: cgrgicak@bu.edu
Fax: +1-617-638-1960

Abbreviations: APH, average peak height within a locus; **AT**, analytical threshold; **EPG**, electropherogram; **IID**, independent and identically distributed; **RFU**, relative fluorescence unit; **SEE**, Simulating Evidentiary Electropherograms; **STR**, short tandem repeat

Colour Online: See the article online to view Figs. 6–8 in colour.

signal from the fluorescently tagged amplicons did not cross threshold.

Previous work has suggested sampling effects, rather than PCR effects, are the chief cause of peak height discrepancies, which are usually measured by the ratio of the peak intensities of the two alleles within a locus [12, 13]. Given that both moderate- and low-template samples are regularly processed, defining the sensitivity of the procedure is required (SWGDAM, 2012. Validation guidelines for DNA analysis methods. http://media.wix.com/ugd/4344b0_cbc27d16dcb64fd88cb36ab2a2a25e4c-.pdf). Specifically, sensitivity studies are used to garner information related to the dynamic range, ideal target level, peak height ratio expectations, signal to noise ratios, and stochastic effects of the assay. Generally, these parameters are established by generating data from a series of DNA samples of varying quantity and of known genotype. Though it is advisable to utilize single-source casework or environmental samples to characterize these parameters, there are uncertainties associated with employing unknowns during validation; namely, the number of contributors and the genotypes of said contributors are unknown. Accordingly, the validation dataset is typically generated by obtaining DNA from known sources where there are ample copies of DNA. To produce validation samples with low-copy numbers, the extract may be quantified and then serially diluted. Since low-template samples obtained from the environment are unlikely to be serially diluted in this way, a study that explores differences between data originating from true low-template samples and manufactured low-template samples is warranted but difficult to design since it necessitates the transfer of one or a few cells by way of single-cell manipulation techniques [14, 15].

In principle, PCR coupled with CE and fluorescence detection is sensitive enough to distinguish allele response from noise. If true, then an increase in injection time or voltage [16], additional PCR cycles [2, 17], or implementation of post-PCR clean-up processes [18] can all play important roles in ensuring all signal that can be detected is detected. Decreasing the AT to a level that assures reasonable protection from labeling noise while simultaneously ensuring good allele detection rates has also been explored [19] and may be a sensible option. Each of these modifications, however, requires additional cost or effort if they are to be successfully implemented within the laboratory. For example, post-PCR clean-up methods require additional reagents and labor, while decreasing the AT may result in labeling of artifactual peaks, such as pull-up or double-back stutter, that would require additional manpower or software implementations to analyze and interpret. Furthermore, designing wet-laboratory experiments to test the viability of introducing new laboratory processes is costly and requires the amplification and analysis of many samples that may not be readily available.

STR-based EPG signal is also encumbered by a common PCR artifact known as stutter [20]. As with instrument noise, it is difficult to distinguish stutter from allele signal in mixtures, particularly when only a few template copies of DNA are collected from one or more contributors. In the past, stutter ratios, which are usually determined by dividing the signal of the stutter peak by the signal strength of the allele peak, were calculated from a set of standards with the goal of establishing and implementing stutter thresholds designed to filter potential stutter. Filtering peaks in stutter position is, however, no longer recommended since the peak in stutter position may have allelic signal contained in it [21, 22]. Consequently, modern interpretation strategies have implemented stutter models to probabilistically evaluate these peaks [3, 23–25], and models describing stutter at high template levels (typically > 0.4 ng) have been described elsewhere [2, 26–29]. In general, amplification of normal amounts of DNA results in stutter peaks that tend to be less than 15% [30], but if the DNA concentration is in the low-copy regime, slippage that occurs in early cycles can result in stutter peaks that are proportionally larger and can be greater than the allelic peak. Since forensic laboratories are processing DNA from touched samples, which in all likelihood contain only few copies of DNA, characterizing and exploring the stutter ratio at low- and single-copy levels is warranted.

For these reasons, it would be useful to analyze EPG data where the noise, allele, and stutter signal are isolated. Generating and evaluating experimental data pertaining to the noise, allele and stutter is preferred, but it is difficult to isolate these components using wet-laboratory techniques. Moreover, generating well-defined extracts containing known copy numbers is a significant challenge. Thus, modeling the entire forensic laboratory in silico based on a data-driven parameterization and then generating synthetic EPGs is a useful method to understand the impacts of processing decisions on the final EPG and explore the origins of variation observed in the signal.

Models that synthesize allele signal generated from stochastic variation induced by the PCR process [31, 32] as well as the fuller laboratory process [2] have been described. That work is extended here by incorporating aspects of the forensics process that are particularly significant in either the low- or multi-copy regimes. These include the following: (i) quantification and sampling that occur pre-PCR; (ii) amplicon-number dependent PCR efficiency; and (iii) the inclusion of instrument noise.

An implementation of the full model, named SEEIt (SEE refers to Simulating Evidentiary Electropherograms), can be downloaded from http://sites.bu.edu/grgicak/software/. In its current form, the model has been developed in the Stella environment and requires a licensed version of Stella (iseeSystems.com); development of the SEEIt model in multiple environments is possible and is anticipated. The publically available version of SEEIt incorporates up to six individuals, but for exposition we present the single-source dynamic model and concentrate on data generated from a D8S1179 locus model parameterization. We illustrate the model's utility by exploring allele dropout, peak heights, peak height ratios, and stutter behavior within the single- and multi-copy number regimes.

2 Materials and methods

Building upon the work presented in [2], a mechanistic laboratory model of forensics EPG creation and analysis was developed. The model consists of three modules: (i) the pre-PCR component, which includes quantification, dilution of extract (if desired), and PCR setup; (ii) PCR; and (iii) CE and fragment analysis. The rational for each modeling choice is explained at each stage. After the model pieces are introduced, a description of the data-driven parameterization of each module that is contained in the software implementation is provided. In terms of notation, each bold symbol corresponds to a user-defined input, which can be altered in line with a particular laboratories protocol or to explore the consequences of procedural changes. The symbol $\sim$ indicates equality in distribution.

2.1 A mechanistic model of the forensics process

2.1.1 Module 1: Quantification, dilution of extract, and PCR setup

Initial inputs to the model include the average concentration of DNA, μ_{DNA} ng/μL, which can be based, for example, on qPCR or UV-Vis quantification expectations [33–35], as well as the percentage RSD (Relative Standard Deviation) of the quantification value, α_{DNA}. Capturing extraction variability, the concentration of the DNA, D ng/μL, in the extract is modeled as a normal random variable with those parameters, $D \sim \text{Normal}(\mu_{DNA}, (\alpha_{DNA}\,\mu_{DNA})^2)$.

The sampled concentration is converted to a total copy number, T, for each allele, a, by assuming 6.3 pg of DNA per diploid cell [36], and multiplying D by the total extract volume, V_{tot} μL, obtaining $T = \lfloor D V_{tot} 10^3/6.3 \rfloor$, where $\lfloor x \rfloor$ indicates the greatest integer that is less than or equal to x. From the total extract volume, an aliquot, $V_{aliquot}$ (μL), of the extract can be directly added to the PCR, or can undergo up to three serial dilutions. Here, $V_{aliquot}$ is a random variable, again described using a Normal distribution with nominal volume, $\mu_{aliquot}$(μL), bias, $\beta_{aliquot}$ (μL), and variance, $\sigma^2_{aliquot}$ (μL)^2,

$$V_{aliquot} \sim \text{Normal}\left(\mu_{aliquot} + \beta_{aliquot}, \sigma^2_{aliquot}\right). \quad (1)$$

If no dilutions are performed, assuming that the sample is well mixed, a copy of each individual allele, a, is randomly selected independently with probability $V_{aliquot}/V_{tot}$. This results in the total initial copies of the allele, T_0, that shall undergo amplification being captured by a binomial random variable

$$T_0 \sim \text{Binomial}\left(T, \frac{V_{aliquot}}{V_{tot}}\right). \quad (2)$$

If dilutions are performed, then $V_{aliquot}$ is sampled from V_{tot} as described by Eqs. (1) and (2), but buffer is added to the aliquot, and another aliquot sampled independently from the resulting mixture. This procedure is repeated in the case of serial dilutions. To capture variability in pipetting, the added buffer volume, B, is itself described as being normally distributed with specified mean, μ_{buffer}, bias, β_{buffer}, and variance, σ^2_{buffer},

$$B \sim \text{Normal}\left(\mu_{buffer} + \beta_{buffer}, \sigma^2_{buffer}\right). \quad (3)$$

Thus, this first module models the pre-PCR procedures leading to the pre-PCR copy number of each allele at each locus.

2.1.2 Module 2: PCR

Alleles that survive the pre-PCR process undergo amplification. Akin to the PCR model in [2], we use a multitype Galton–Watson process [37] to capture stochastic PCR processes, but with two differences. First, the possibility that stuttered copies stutter further is included. In [2] the copying efficiency of PCR, E, the probability that an amplicon is duplicated per round, is modeled as constant. While that is a good approximation for low starting template, PCR is well known to become less efficient as more amplicons are produced [5], which influences artifacts such as stutter. Thus, the second modification is the inclusion of an amplicon number dependent PCR efficiency in the model. With N_c denoting the total number of amplicons in the PCR, true plus stuttered from a given locus, at the end of cycle c, each allele is duplicated in cycle c with a probability $E(N_c)$, where E is a decreasing function of the number of amplicons present at the end of cycle c. A data-driven characterization of $E(N_c)$, which is implemented in the software, is explained in Section 2.2.2 below. At each round of amplification, each true amplicon independently has a probability, π_{S1}, of stuttering while each stutter product stutters further still with probability π_{S2}. Note that duplication of amplicon fragments does not occur until the third cycle of the PCR [5], which is also captured in the model.

Recall that T_0 is the initial number of copies of allele a, as determined by Module 1. After c rounds of amplification, let T_c denote the number of true amplicons and S_c denote the number of stuttered amplicons. A mathematical description of the PCR starts with $T_2 = T_0$ and $S_2 = 0$, and for $c \geq 2$ we have the following stochastic recursions describing the growth of these coupled quantities:

$$T_{n+1} = T_n + \sum_{i=1}^{T_n} C_i^{c,T}\left(1 - D_i^{c,T}\right) \quad (4)$$

and

$$S_{n+1} = S_n + \sum_{i=1}^{Tn} C_i^{c,T} D_i^{c,T} + \sum_{j=1}^{S_n} C_j^{c,S}(1 - D_j^{c,S}), \quad (5)$$

where $C_i^{c,T}$and $C_i^{c,S}$ are independent and identically distributed (IID) Bernoulli random variables that take the value 1 (indicating a successful copy) with probability $P(C_i^{c,T} = 1) = E(N_c)$ which captures copying efficiency, and the value 0, indicating no copy is produced, with probability $P(C_i^{c,T} = 0) = 1 - E(N_c)$. The $D_i^{c,T}$ are also IID Bernoulli random variables that take the value 1 with

probability $P\ (\ D_i^{c,T} = 1) = \pi_{S1}$, describing a stutter from true to $n-1$, and 0, corresponding to no stutter from true to $n-1$, with probability $P\ (\ D_i^{c,T} = 0) = 1 - \pi_{S1}$. Finally, the $D_i^{c,S}$ are IID Bernoulli random variables with $P\ (\ D_i^{c,S} = 1) = \pi_{S2}$ capturing the possibility of stutter on stutter.

Equations (4) and (5) can be understood in the following terms; at each round all previously created true and stutter amplicons are preserved. Each true amplicon is copied with probability $E(N_c)$ and with probability $1 - \pi_{S1}$ it does not stutter, producing an additional true amplicon in the next round. As well as the previous round's stutter amplicons, each true amplicon that is replicated but stutters creates a new stutter amplicon and, moreover, each existing stutter amplicon can be replicated and, so long as the replicate does not stutter further, a new stutter amplicon is created.

The total number PCR cycles is a model input, $N_{\mathbf{PCR}}$, and may be 27, 28, or 29 cycles in forensics applications [38]. In software terms, the total number of amplicons (true and stutter) produced during each cycle "flow" into stocks, which are designated in the causal-loop diagram (Fig. 1) by a solid border. The resultant allele and stutter amplicon count for each allele is exported to Module 3—the module in which the allele designations and the relative fluorescence unit (RFU) peak heights are assigned to the amplicons. By designing the model in this way, the information stored in the stocks and flows can be readily tabulated and evaluated for all cycles.

2.1.3 Module 3: CE and genotype assignment

For each STR locus l, the population frequency of each allele a is a model input, f_a^l. Each of the two alleles at each locus is assigned independently via a multinomial distribution described by those frequencies, $A_l \sim \mathit{Multinomial}(\{f_a^l\})$, with the stutter position defined to be one repeat unit shorter. Thus, we obtain a collection of allele pairs for each locus, which are randomly assigned to the amplicon output of the stochastic PCR process, $T_{N_{PCR}}$ and $S_{N_{PCR}}$. Lastly, we convert the number of true and stutter amplicons into an RFU value by assuming a constant fluorescence per amplicon, $\boldsymbol{\alpha}$, known as the CE sensitivity. The data-driven characterization of $\boldsymbol{\alpha}$ included in the software is provided in Section 2.2.3 below.

Noise is an inherent instrument issue that, according to a recent study [39], occurs at approximately 15% of allelic positions, and when it occurs is best described as a log-normal distribution. Log-normal distributions are more prone to large outliers than normal distributions and can generate noise that is of similar peak height to true and stutter products in the presence of low starting template or less numerous rounds

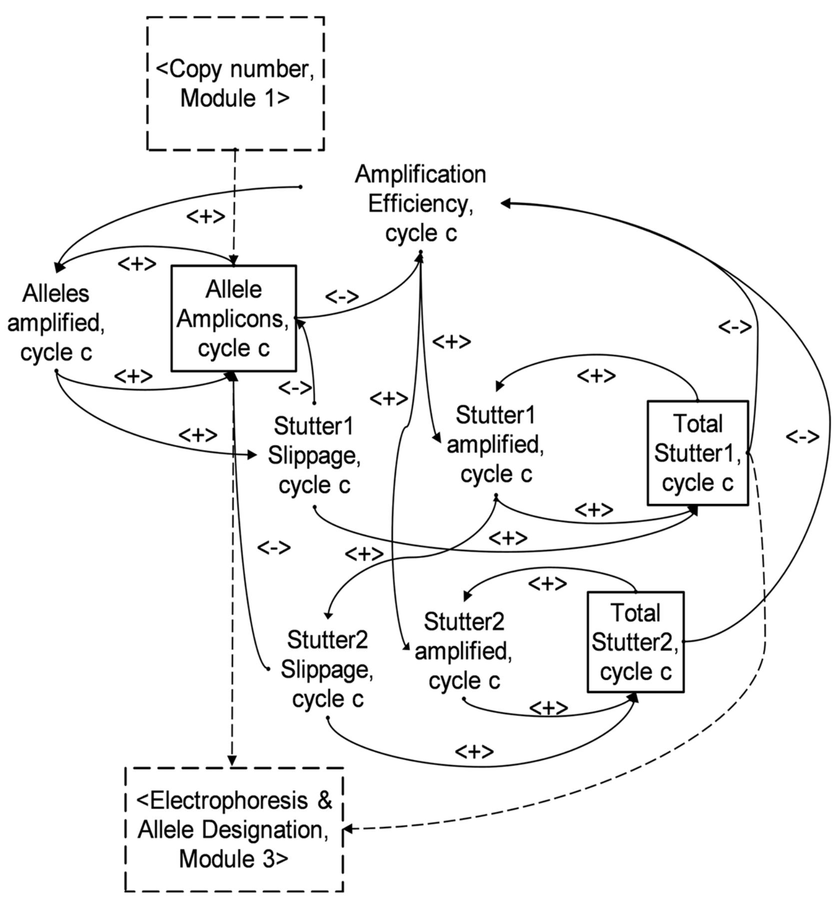

Figure 1. Causal loop-diagram of the PCR module (Module 2) showing the different variables in the system and the ways in which they are related. As the total number of allele, stutter 1 ($n-1$) and stutter 2 ($n-2$) amplicons grows, the amplification efficiency, $E(N_c)$, decreases, thereby reducing the number of amplicons successfully amplified.

of PCR, N_{PCR}. For the model, we incorporate the finding by independently adding noise at each allelic position with probability 0.15, whereupon it follows a log-normal with a per-locus mean, μ_{noise}, and variance, σ^2_{noise}, taken from [39]. If noise occurs at a position assigned to true or stuttered alleles, its fluorescence is treated as additive.

The final genotype contains signal from a combination of noise, stutter, and allele, and the RFU from each component is added to obtain the final peak height for each allele position or "bin." With two alleles, A_l^1 and A_l^2, giving rise to true and stutter amplicons ($T^1_{N_{PCR}}$, $S^1_{N_{PCR}}$) and ($T^2_{N_{PCR}}$, $S^2_{N_{PCR}}$) respectively, at locus l, the final observed fluorescence at allele a is

$$F_a = \sum_{i=1}^{2} \left(1_{\{A_l^i = a\}} T^i_{N_{PCR}} + 1_{\{A_l^i = a+1\}} S^i_{N_{PCR}} \right) \alpha + X^l_a \,, \qquad (6)$$

where $1_{\{A_l^i = a\}}$ denotes the indicator function, which takes the value 1 if $A_l^i = a$ and 0 otherwise, while for each l and an X^l_a is an independent random variable that with probability 0.85 is zero and with probability 0.15 is lognormally distributed with mean μ_{noise} and variance σ^2_{noise}.

2.1.4 Model integration and display

For the software realization of the model, the output on the interface includes the following: (i) the initial copy number for each allele for all loci; (ii) the number of DNA copies produced during PCR; (iii) the known genotype of each contributor; (iv) PCR efficiency at each cycle; (v) the final profile, which includes signal from noise, reverse stutter and alleles; and (vi) the noise contribution. Other values that are stored and are accessible include, but are not limited to, the number of stutter products produced at each cycle of the PCR, number of amplicons aliquoted into the CE sample plate for injection, and volume of liquid aliquoted during any of the steps.

2.2 Data-driven model parameterization

The model described above requires several inputs, recapitulated in Table 1, that need to be specified. To most accurately capture the experimental process, we provide a description of a parameterization of the more involved components taken from data generated in our laboratory, including the CE sensitivity, $\boldsymbol{\alpha}$, and the amplicon number dependent PCR copying efficiency function, $E(N)$. These are included in the software implementation of the model.

2.2.1 Parameterizing module 1

Module 1 simulates the PCR set-up process, which includes quantification of the DNA extract, extract dilution, and PCR setup. This concentration value is taken to be an accurate representation of the bulk concentration of DNA in solution. The extract volume is an important quantity in the model as it is used to determine the number of target molecules, T, aliquoted from extraction tube to PCR or dilution tube. The extract volume can range from 10 to 200 μL, which are typical extract volumes used in forensic laboratories [40,41]. Extracts can be serially diluted, and the maximum pipette volume is 1000 μL for both $\mu_{aliquot}$ and μ_{buffer}. Last, the maximum volume of DNA that can be transferred into the PCR tube is 10 μL as described in [30]. All pipette biases and SDs (standard deviations) cannot exceed the maximum volume transferred, (i.e., $\mu_{aliquot}$ and μ_{buffer}) or 100 μL. Though a 100 μL pipette bias or SD is extreme, particularly when compared to the ISO standards (ISO/IEC 17025:2005(E) 2005) for testing and calibration laboratories, the ability to test different quality control failure scenarios in an operations setting is warranted from a training, quality control, and quality assurance perspective.

2.2.2 An empirically derived model of amplicon number dependent PCR efficiency

To create a functional description for the PCR efficiency, $E(N)$, we estimated the change in efficiency with total amplicon number by utilizing empirical qPCR data from this laboratory. Though many kinetic models of the PCR process have been previously described [42–46], the exact concentrations of STR amplicons, primers, and active enzyme in forensic human identity kits are unknown, making it a challenge to develop a detailed kinetically based representation of the forensic PCR process. Accordingly, we utilize empirical data generated using the methods described in [47] to approximate the following: (i) the PCR efficiency at early cycles, and (ii) the decrease in efficiency with amplicon level.

The qPCR fluorescence signal of 44 samples from four runs, generated over a period of 6 months, from samples containing 0.42 to 100 ng of DNA were obtained by using the manufacturer's recommended protocol and DNA standard [48]. Using these data, the empirical PCR efficiency for each cycle was determined by

$$E_{qPCR,c} = F_{qPCR,c} / F_{qPCR,c-1} - 1, \qquad (7)$$

where F_{qPCR} is the normalized VIC fluorescence minus the baseline signal generated at a cycle. As we are interested in the efficiency before plateauing, but after $F_{qPCR,c-1}$ is substantially larger than baseline, we take the maximum $E_{qPCR,c}$ obtained from fluorescent signals greater than 0.02. The value of 0.02 was chosen as the minimal distinguishable signal since it was the intensity at which the fluorescence consistently and discernably doubled, indicating reliable and detectable growth of amplicon numbers. The maximum $E_{qPCR,c}$ per sample ranged from 0.7 to 1.0, with a median of 0.96, indicating that the PCR is highly efficient in the low-amplicon concentration range. This is larger than the PCR efficiency reported in [2], but correlates well with the slopes obtained from our qPCR standard curves throughout the past 3 years, which range from –3.311 to –3.582 and correspond to efficiencies between 0.90 and 1.0. Thus, at these low cycle numbers we use a constant efficiency of $E_0 = 0.96$ to obtain a

Table 1. Extract volume, pipette, PCR, allele frequencies, and capillary sensitivity parameters used in Simulations 1 through 6.

Parameters held constant during all simulations						
	Extract volume, V_{tot} (μL) = 50	Percentage RSD of DNA concentration, α_{DNA} = 0%	Initial PCR efficiency, E_0 = 0.94	Nominal volume of CE aliquot, μ_{CE} (μL) = 1	Allele frequencies, f_a^l = [30]	
Parameters modified between simulations						
	Simulation 1 (*Sim* 1)	Simulation 2 (*Sim* 2)	Simulation 3 (*Sim* 3)	Simulation 4 (*Sim* 4)	Simulation 5 (*Sim* 5)	Simulation 6 (*Sim* 6)
Concentration of DNA, μ_{DNA} (ng/μL)	0.00078	780	0.0078	0.0078	0.0078	0.25
Nominal volume of DNA into dilution, $\mu_{aliquot}$ (μL)	0	1	0	0	0	0
Nominal volume of buffer, μ_{buffer} (μL)	0	999	0	0	0	0
Number of serial dilutions	0	2	0	0	0	0
Nominal volume of DNA into PCR, $\mu_{aliquot,PCR}$ (μL)	10	10	1	1	1	1
PCR cycle number, N_{PCR}	29	29	28	29	29	29
CE sensitivity, α (RFU/amplicon)	4.07×10^{-7}	4.07×10^{-7}	4.07×10^{-7}	4.07×10^{-7}	8.12×10^{-7}	4.07×10^{-7}

All pipette biases ($\beta_{aliquot}$, β_{CE}) and SDs ($\sigma_{aliquot}$, σ_{CE}) were set to 0 and all extract volumes (V_{tot}) were set to 50 μL. The stutter slippage probability was set to 0.0055.

relationship between the qPCR (i.e., VIC fluorophore) signal and the nominal number of amplicons produced at cycle c:

$$N_c = N_o\ (1 + E_0)^c = N_o\ (1.96)^c, \tag{8}$$

where

$$N_0 = 2M_{DNA} \big/ \left(6.3\ \ 10^{-3}\right), \tag{9}$$

the factor 2 is implemented because there are two copies per cell, and the mass of DNA standard, M_{DNA} (ng), is provided by the manufacturer [48]. We plot N_c versus the VIC signal at maximum $E_{qPCR,c}$ for each sample. Figure 2A demonstrates there is a direct proportionality between the signal obtained from the exponential segment of the PCR curve and the nominal concentration, with a slope of 1.93×10^{-12}. This slope is used to approximate the number of amplicons produced in the linear and plateau phases that, in turn, aid in estimating the efficiency with respect to total product levels. Figure 2B is a plot of the efficiency as determined by qPCR fluorescence, Eq. (7), with respect to N_c, the total number amplicons at cycle c. An exponential function was fit to the data using the least squares fit functionality in Igor Pro version 6.1.2.1. We see that the PCR efficiency, $E_{qPCR,c}$, is approximately 1 when the amplicon numbers are less than 10 billion. As the reaction progresses, the number of amplicons quickly grows. As a result, the efficiency quickly approaches 0 at later cycles—when the amplicon numbers are large. For purposes of characterizing the efficiency as a function of amplicon number, $E(N_c)$, we incorporate this change in efficiency per cycle, c, into the dynamic model as

$$E(N_c) = E_0\ \ e^{-1.12 \cdot 10^{-12}(N_c)}, \tag{10}$$

where E_0 is the baseline efficiency. In the code, this functionality may be turned off, if desired, in favor of a constant efficiency as in [2].

2.2.3 CE sensitivity, that is, fluorescence per amplicon, α

To obtain a reasonable CE sensitivity, α, the nominal DNA amplicons of a set of single-source standards ranging in target from 0.016 to 0.5 ng, amplified using the Identifiler Plus kit was plotted against the RFU of the locus (Fig. 3). Although amplification was for 29 cycles, the first two cycles do not produce fully formed fragments [5] and to account for this phenomenon we subtract 2 from the total cycle number in computations. If the amplification efficiency of the target is consistently 96% and it is assumed that RFU is directly proportional to the concentration of amplified product after 29 cycles, the following linear relationship should result:

$$\text{RFU} = \alpha\ N_0\ 1.96^{27} + A = \alpha N_{29} + A, \tag{11}$$

where A is the y-intercept, which one would expect to be 0 if the proportionality is unbiased.

Thus, if optimal conditions exist, a plot of $N_0\ 1.96^{27}$ versus peak height (RFU) should result in a straight line. The resultant slope is the CE sensitivity and represents the increase in RFU signal per amplicon produced, α. For this computation, N_0 was calculated using Eq. (9).

CE sample preparation steps are modeled as described in Module 1. Briefly, μ_{CE}, β_{CE}, and σ^2_{CE} are the nominal

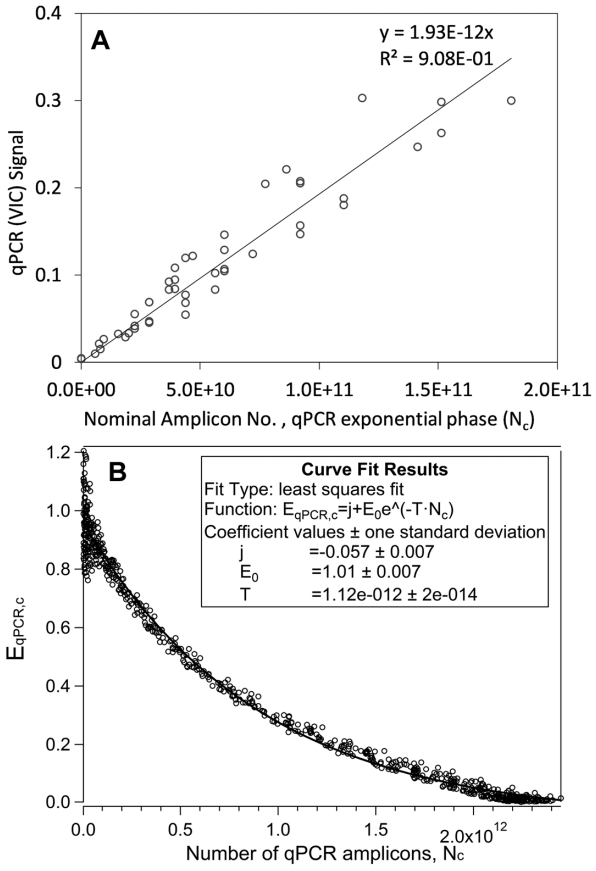

Figure 2. (A) qPCR VIC fluorescence obtained from a set of DNA standards containing 0.42 to 100 ng versus the nominal amplicon number as determined by Eq. (8). (B) The empirical efficiency as determined by Eq. (7) versus the number of qPCR amplicons produced during 40 cycles of qPCR using the Quantifiler Duo quantification kit and the least-squares exponential fit to the data.

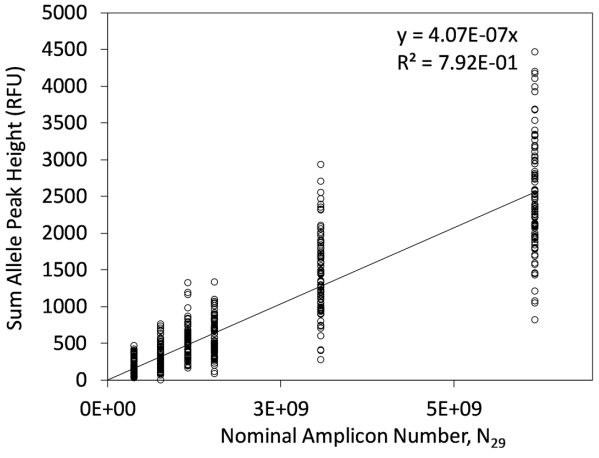

Figure 3. The sum of the allelic peak heights (RFU) for the D8S1179 locus obtained when 0.016, 0.031, 0.047, 0.063, 0.0125, and 0.25 ng of DNA was amplified using the AmpFISTR Identifiler Plus amplification kit (29 cycles). STR fragment separation was achieved with a 3130 Genetic Analyzer. The nominal amplicon number at cycle 29, N_{29}, was calculated using Eq. (8).

volume, pipette bias, and pipette variance associated with the CE sample preparation. V_{CE} is the volume of sample aliquoted during CE preparation and is described using a normal distribution. The number of amplicons that undergo electrophoresis is a binomial random variable where the PCR reaction volume is set to 25 μL.

2.3 Parameterization of simulations reported on in this paper

Six distinct simulation scenarios were used for the analysis in Section 3. Table 1 shows the input parameters for each. In all cases, the pipette biases and variances were zero. An extract volume of 50 μL was chosen as it is one of the recommended elution volumes for silica-based extractions of forensic samples [40]. The baseline PCR efficiency was set to 0.94, which is the average PCR efficiency from calibration standards obtained in this laboratory over the last 3 years, corresponding well to the median efficiency (i.e., 0.96) obtained from the raw qPCR analysis of 44 samples described in Section 2.2.2.

2.4 Low-template laboratory empirical data generation

Single-source profiles were obtained by extracting DNA from whole blood or proficiency test samples purchased from various manufacturers using phenol/chloroform purification and alcohol precipitation. The extracts were quantified using Quantifiler Duo (Life Technologies, Carlsbad, CA, USA) on the Applied Biosystems 7500 (Applied Biosystems, Foster City, CA, USA) using the manufacturer's recommended thermalcycling protocol and a validated, universal calibration curve [47]. The samples were amplified on the GeneAmp PCR Amplification System 9700 using AmpF*l*str Identifiler Plus (Life Technologies) following the manufacturer's recommended protocol (29 cycles) at 0.0078 ng [30]. Thus, a total of 95, 0.0078 ng single-source amplified samples were generated. All samples were injected for 5, 10, and 20 s at 3 kV on the Applied Biosystems 3130 Genetic Analyzer, and resultant EPGs were analyzed with GeneMapper ID-X v1.1.1 (Applied Biosystems) at 1 RFU. Artifacts such as pull-up, complex pull-up, and minus A were manually removed. Pullup was defined as a peak that appears in the same position (±0.3 bases) as an allelic peak in another color channel and has a peak height of 5% or less of the allelic peak. Complex pullup was defined as a peak with a plateau-like shape located between two adjacent allelic peaks in a different color channel. Minus A was defined as a peak one base shorter in size (±0.3 bases) than an allelic peak. There were no height restrictions for the complex pull-up and minus A artifacts. The filtered genotype table for each sample was exported from GeneMapper ID-X for downstream analysis.

3 Results

To illustrate the model's utility, we used it to investigate three important aspects of the laboratory process that would be

challenging to assess experimentally: First, the impact of serial dilution on dropout; second, the impact of cycle number and injection time on peak height; and finally, the impact of low-template DNA levels on stutter ratios.

3.1 Peak height variations and allele dropout from diluted and undiluted samples

To obtain single-source validation samples with low-template levels, an extract containing ample copies of DNA may be serially diluted in order to reach low-template levels [12, 49, 50]. Therefore, it is of interest to study the effects of serially diluting concentrated DNA stocks on the EPG and to examine if peak height variability obtained from diluted samples would be representative of the variability seen in low-template samples that do not undergo such processing. To examine this 2000 undiluted (*Sim* 1) and 2000 diluted (*Sim* 2) heterozygous pairs were simulated (Table 1). Figure 4A shows the RFU of the high molecular weight peak, H_{a2}, plotted against the RFU of the low molecular weight peak, H_{a1}, using heterozygous pairs from *Sim* 1 and 2. The tallest heterozygous peak with a sister allele that did not survive the pre-PCR sampling process for undiluted samples was 101 RFU, while the tallest surviving sister peak height for diluted samples was 147 RFU. Figure 4A also shows that the data cluster in groups, where the most pronounced groups are centered at (25, 24), (23, 47), (48, 23), and (47,46), regardless of whether or not the samples were diluted. We further explore the impact of diluting concentrated extracts to reach the low-template regime by examining the heterozygous balance within a locus, defined as,

$$\mathrm{Hb} = H_{a1}/H_{a2}\,, \tag{12}$$

where H_{a1} is the peak height of the first allele at D8S1179, and H_{a2} is the height of the second allele.

Figure 4B is a plot of the logarithm of Hb versus the average peak height (APH) of the two alleles that survived pre-PCR sampling. Peak height balance has been previously studied [27, 51, 52], and it has been suggested that variability in Hb proportionally decreases with APH as

$$\mathrm{var(Hb)} = (\sigma^2_{\mathrm{PH}})/\mathrm{APH}. \tag{13}$$

In the case of these low-template sample simulations, the APH for *Sim* 1 and 2 were 37 and 39 RFU, respectively. Using the estimated var(Hb) from the simulations in conjunction with Eq. (13), it was determined that σ^2_{PH} increased from 37.8 to 43.3 for *Sim* 1 and 2, respectively. Taken together, these results suggest a small but real effect associated with diluting extracts containing large copy numbers in order to manufacture samples that contain few copies of DNA.

For well-mixed solutions, sampling due to dilution is accurately described by binomial probabilities, as in Eq. (2), making it particularly amenable to mathematical analysis. For example, mathematically, the outcome of serial dilution is identical to a single dilution with a sampling probability that is the product of sampling volumes. Moreover, the probability of dropout can be readily computed and so can be considered over a wide range of dilution factors. Striving to obtain a sample containing 7.8×10^{-4} ng/μL of DNA, such that 10 μL of this solution will result in approximately one copy of DNA to undergo PCR, we can compute the probability that zero copies survived the pre-PCR sampling process for a given dilution factor. Recall that the average copy number is $T = DV_{\mathrm{tot}}\,10^3/6.3$ and so in this example $(7.8\ 10^{-4})(48\ 10^3)/6.3 = 5.94 = 5$. Note that 48 μL stems from the knowledge that typically 2 of 50 μL of the extract is utilized to quantify during PCR [48], which is implemented in the software. Therefore the probability of obtaining zero copies for a given dilution factor, r, is

$$\begin{aligned}&\mathrm{P}\ (\mathrm{Binomial}\ (\lfloor 5.94\,r\rfloor,\ 10/(48\,r)) = 0)\\ &\quad = (1 - 10/(48\,r))^{\lfloor 5.94\ r\rfloor}.\end{aligned} \tag{14}$$

When $r = 1$, there is no dilution. As r becomes larger, the starting density is higher and the sampling probability is proportionally lower, ensuring the same average outcome.

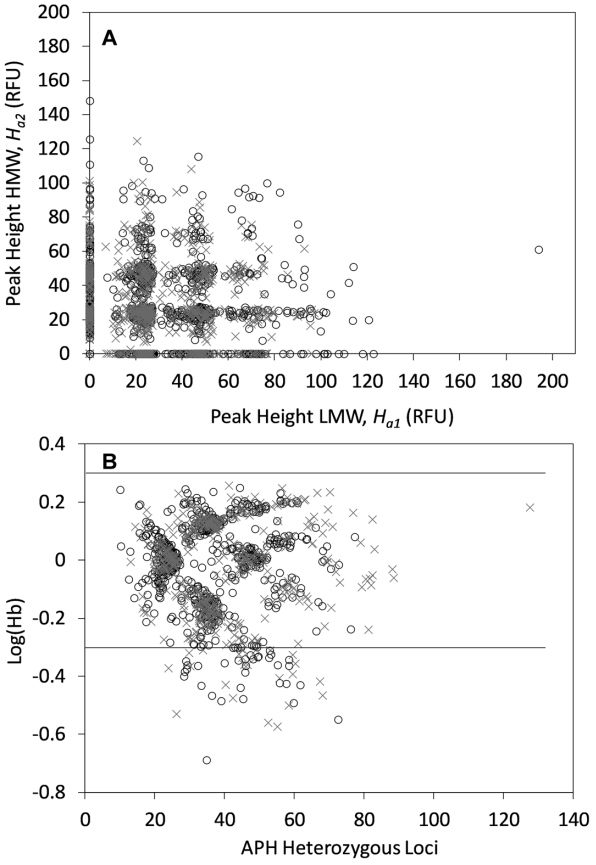

Figure 4. (A) The peak height of the high molecular weight allele, H_{a2}, versus the peak height of the low molecular weight allele, H_{a1}, for 2000 simulated samples of 0.0078 ng and (B) the logarithm of the peak height balance (Hb) against the average peak height for (x) undiluted and (○) diluted samples. The two horizontal bars in (B) represent heterozygote balance of 50%.

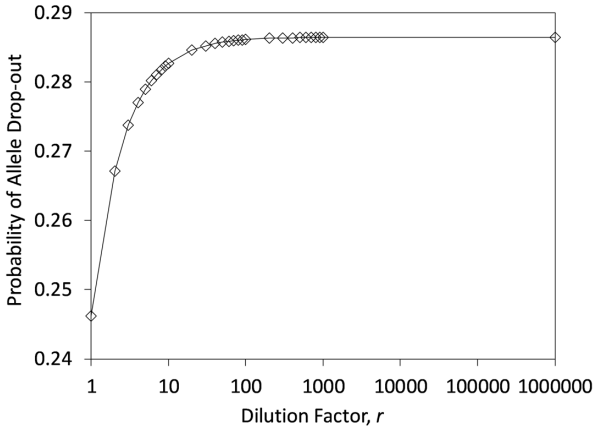

Figure 5. The probability of allele dropout with respect to dilution factor, *r*, for a sample containing $\lfloor 5.94r \rfloor$ copies of DNA at the start of sampling. A dilution factor of 1 denotes no dilution takes place between quantification and amplification.

The rate of allele dropout as a function of the dilution factor, *r*, is presented in Fig. 5, which illustrates that the likelihood an allele survives the pre-PCR sampling process is dependent upon whether or not the extract was diluted prior to amplification. Indeed, Fig. 5 demonstrates there is an increasing likelihood of dropout as *r* increases, which converges to a limit. When $r = 1$, Eq. (14) gives a drop-out probability of 0.246, while analysis using L'Hopital's Rule shows that for large *r* this probability converges to $e^{-5.94^{10}/_{48}} = 0.29$. While one can assess this mathematically as described, one of the merits of the model is that this effect can also be seen directly from simulations without recourse to mathematics. When we examine the allele drop-out rate in *Sim* 1 and *Sim* 2, for example, we find that the number of alleles that dropped out increased from 485 (24.25 ± 0.9% SEM) to 575 (28.75 ± 1% SEM) for the undiluted and diluted samples, corresponding well to the values determined mathematically.

From a validation perspective, these results suggest that allele detection rates of low-template DNA samples garnered from diluting extracts with large quantities of DNA do not equal the detection rates of low-template samples that do not undergo dilution. However, we note that it is not always the case that DNA from low-template contributors will not undergo dilution. For example, in a forensic casework scenario, a two-person major–minor sample containing large quantities of major may, indeed, require dilution. There are innumerable scenarios that lead to various processing decisions in the laboratory. This analysis suggests that diluting a few very concentrated extracts in an attempt to mimic low-template or 'touch' samples is not ideal. Rather, production of a sufficient validation dataset generated using representative and typical laboratory processes is the preferred mechanism by which to establish the limitations of a method and, subsequently, the peak height ratio expectations, stochastic effects and signal to noise of the assay.

3.2 Effects of cycle number and injection time on peak height

Recently, a number of studies have focused on characterizing noise generated during the forensic PCR process [39,53]. This is typically performed in order to establish an AT, which is a signal threshold designed to filter noise. Since there is a trade-off between signal loss and false noise detection associated with the AT, it is arguably one of the most important analysis parameters set by the laboratory [20]. Ideally, the separation between noise and allele signal should be substantial enough to distinguish noise from the signal obtained from one copy of DNA.

In Fig. 6A is plotted the histogram of peak heights when 100 000 profiles were simulated with the cycle number, N_{PCR}, set to 29. The nominal input value of DNA, μ_{DNA}, was 0.0078 ng/μL and we aliquot 1 μL (i.e., ~1 copy) into the PCR reaction. Other details of the simulation can be found in Table 1 under column *Sim* 4. The PCR efficiency was set to be amplicon number independent, $E = 0.94$, the stutter slippage probability was $\pi_{S1} = \pi_{S2} = 0.0055$ for the D8S1179 locus, which is larger than the 0.002 estimate in [2], but is in

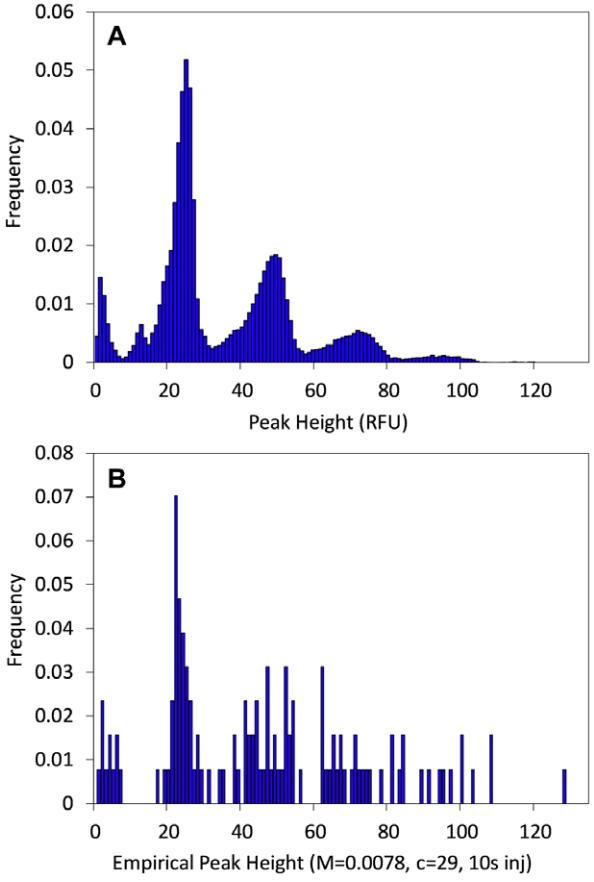

Figure 6. Histograms of peak heights generated from (A) 100 000 simulations using the model and parameter set *Sim* 4, and (B) experimental data from amplicons ($n = 82$) with target mass of 0.0078 ng, amplified for 29 cycles and injected for 10 s.

line with 0.005 used in [32]. Figure 6A demonstrates that a multimodal pattern with the first, second, third, and fourth peaks centered at 3, 26, 49, and 75 RFU, respectively, was obtained. Figure 6B displays the peak height histogram of 82 heterozygous D8S1179 pairs from low-template samples generated in this laboratory using conditions described in Section 2.4. Only heterozygous pairs where the known alleles were at least three STR units apart, to eliminate any impact of stutter effects, are depicted in Fig. 6B. Qualitatively, we see the empirical data has a multimodal pattern that is similar to the simulated data, with the first two peaks centered on 3 and 23. It is difficult to discern the presence of the third and fourth peaks in the empirical dataset due to low sample numbers. Despite this, the presence of similar patterns in both the simulated and experimental data suggests the model generates RFU values consistent with those derived in the laboratory.

We repeat the simulations using the same parameters as describe for *Sim* 4, but change the cycle number to $N_{PCR} = 28$ cycles (*Sim* 3). In addition, we perform a fifth set of simulations using $N_{PCR} = 29$ cycles and doubling the sensitivity from $\alpha = 4.07{\cdot}10^{-7}$ to $8.14{\cdot}10^{-7}$ (*Sim* 5) to mimic laboratory scenarios where the injection time is doubled or the instrument is twice as sensitive. Figure 7A–C present boxplots of *Sim*s 3–5 and summarize the peak height outputs for each simulation against the starting copy numbers, T_0.

Though the increase in injection time and amplification cycle number does not seem to improve the sensitivity (i.e., a difference of approximately two copies is needed to observe discernable changes in signal), the data in Fig. 7 demonstrate there is improved separation between the noise and signal as the cycle number and sensitivity increase. This makes sense; signal originating from the fluorescence, which is a representation of the number of amplicons injected, is expected to double with twice the injection time, or the addition of one PCR cycle, while the noise signal would only mildly be affected by these laboratory modifications.

Therefore, the entire DNA laboratory process can be optimized to produce high-fidelity EPGs such that all of the alleles that have survived the pre-PCR processes have been amplified to a degree that will lead to detection. These data also imply that coupling the optimized laboratory protocols with a carefully chosen AT may provide appropriate levels of protection against noise detection, while still maintaining high rates of allele detection.

To explore this further, we plot the RFU histograms for zero and one copies of DNA for *Sim* 3–5 (Fig. 8A–C). Figures 8B and C indicate that the noise to signal distributions seem reasonably well separated for *Sim* 4 and 5, suggesting that by using an AT of 12 RFU, an $N_{PCR} > 29$ and an injection time >10 s (or an $N_{PCR} > 30$ with an injection time of 5 s) the laboratory would be reasonably confident that all DNA fragments that survived the pre-PCR steps would be detected. Interestingly, these laboratory conditions differ from the manufacturers recommended protocol which suggests an $N_{PCR} = 28$ or 29 and a 5-s injection time using a voltage of 3 kV [30]. Since good signal to noise is obtained by applying small modifications to the laboratory protocol, these data suggest that major

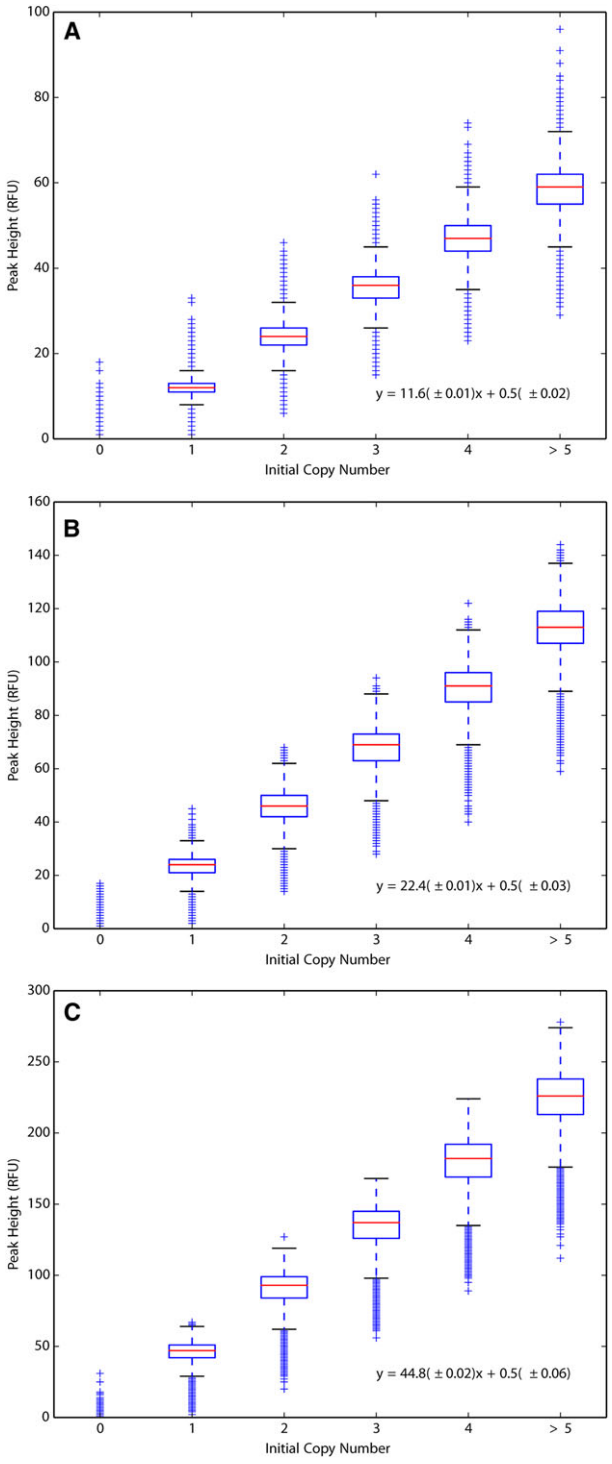

Figure 7. Boxplots of the allele peak height, in RFU, obtained for 100 000 simulations using the parameters described for (A) *Sim* 3, (B) *Sim* 4, and (C) *Sim* 5 in Table 1.

protocol changes, such as the addition of post-PCR clean-up, or the use of multiple injection or amplification protocols, would not likely lead to higher detection rates for samples unperturbed by PCR inhibition or degradation. This corroborates the findings of [2] where it was determined that by using

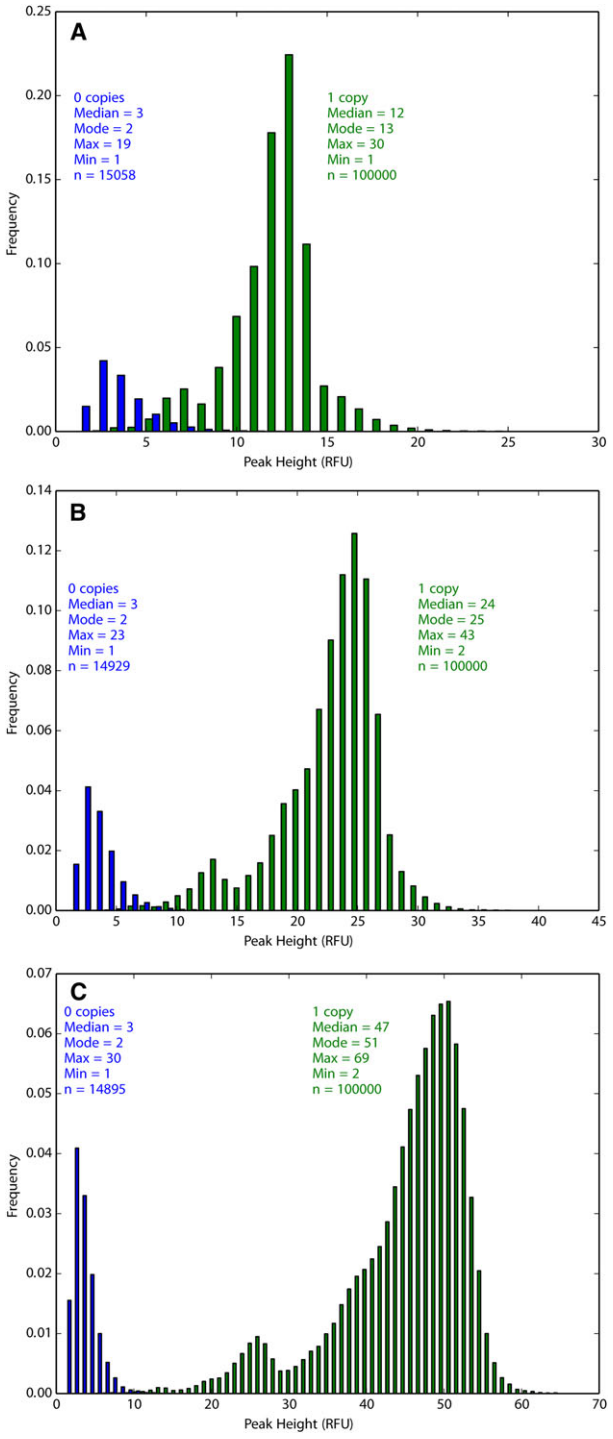

Figure 8. Simulated peak heights (RFU) obtained for (■) noise and (■) one copy of DNA when using parameters described in Table 1 for (A) *Sim* 3, (B) *Sim* 4, and (C) *Sim* 5, for the same starting total copy number, $T = 1$.

$N_{PCR} = 34$ all the alleles that survived sampling crossed the signal threshold of 50 RFU. Similarly, [18] further supports this with empirical studies which demonstrated that for samples amplified using the PowerPlex ESX 16 kit and analyzed using an AT of 50 RFU the number of alleles detected increased as N_{PCR} increased from 30 to 33 cycles; however, no additional alleles were detected with N_{PCR} values of 34 or 35.

Empirical data from this study showed similar results. Samples containing 0.0078 ng of DNA were amplified with the 29-cycle Identifiler Plus protocol and injected using a 5, 10, or 20-s injection time. The number of D8S1179 heterozygous peaks > 12 RFU was determined. Of 94 possible heterozygous alleles, 73, 84, and 84 alleles were detected as the times increased from 5, to 10 and then to 20 s; that is, no additional allele information was gained once the laboratory conditions were modified to an AT = 12 RFU, an $N_{PCR} = 29$ and a 10s/3 kV injection.

Taken together, these studies suggest that, as predicted, PCR coupled with CE is sensitive enough to detect single-copy alleles, if present, and highlights the need to improve the front-end processes affiliated with testing, such as collection, volume transfer, and extraction processes. We note that the laboratory conditions by which we produce these RFU values are not globally applicable and, thus, do not represent recommendations or standards regarding PCR cycle number or injection parameters for all forensic laboratories. Sensitivities are dependent upon the specific laser/detector combination; hence, the sensitivity of each instrument, α, would need to be derived in order to optimize an analytical process within a given laboratory. Instead, a method by which to test numerous laboratory conditions and confirm, through comparison of simulated and empirical data, that the signal-to-noise ratio for one copy is sufficiently large for single-copy DNA analysis is presented. From this, an AT that provides sufficient protection from noise, while ensuring most allele signal is detected, may be acquired. By optimizing the laboratory procedure in this way, both low- and moderate-template samples can successfully be amplified using the same laboratory procedure since both the single- and multicopy signal will be detected using the same laboratory processes. For example, by utilizing an AT = 12, $N_{PCR} = 29$ and a 20 s/3 kV injection, we detected >99.5% of the simulated alleles that survived the pre-PCR set-up stages. Further, at this AT, 99% of the noise peaks fell below this threshold. If more protection against noise is desired such that a larger AT is implemented (i.e., 30 RFU), this model can be used to determine the laboratory parameters that still allow for a 99.5% positive detection rate, provided the allele survived the sampling process.

Visual inspection of the second peak of Figs. 8A–C suggests the peak height distribution from single-copy samples is left-skewed rather than right-skewed as presented in [31]. The difference in the tailing may be explained by the fact that [31] presents an "idealized" model that ignores stutter. As reported in [31], we observe that at moderate copy numbers (i.e., 40), the signal distribution no longer skews to the left or right (data not shown).

3.3 Stutter in the low- and moderate-template regimes

Stuttering that occurs during PCR is a well-studied phenomenon and its mechanistic origins have been proposed

[20]. However, with the introduction of continuous interpretation approaches as a means to compare EPG's from evidence and standards, there has been renewed interest in understanding and characterizing its signal. We supplement this effort by simulating the stutter ratio obtained from single- to moderate-copy numbers in order to evaluate if the distributions used to describe moderate-template samples are well suited for single-copy interpretation.

In advance of considering simulated EPGs, the mechanistic model allows some immediate deductions. From the PCR module alone, one sees that stutter ratios are necessarily more variable at low-template due to the increased likelihood of a significant early stutter event. With higher template these events become increasingly less likely due to the law of large numbers. Beyond that, it can be shown mathematically that in the absence of noise, Pearson's linear correlation between true and stutter fluorescence does not depend on starting template. For low template, this is not observed empirically (data not shown) and explains the need to include noise in the model, particularly at low template. With higher template numbers, signal to noise ratios are such that the noise is an insignificant component. At low template, however, noise can dominate.

We simulated 1000 heterozygous profiles where the alleles were at least two repeat units apart for μ_{DNA} = 0.0078 ng/μL (*Sim* 4) and 0.25 ng/μL (*Sim* 6). These data demonstrate that the stutter ratios for samples containing low levels of DNA are larger and more varied than those obtained from samples containing ample copies of DNA. For example, synthetic EPGs derived from extracts with μ_{DNA}= 0.0078 ng/μL resulted in a mean stutter ratio of 0.103 ± 0.226 with a maximum and minimum 3 and 0, respectively. In contrast, the concentrated samples, where μ_{DNA}= 0.25 ng/μL, resulted in average stutter ratios of 0.071 ± 0.013. We highlight that this model generates signal whereby the final genotype contains signal from a combination of noise, stutter, and allele, as described in Eq. (6). Thus, the RFU from the noise component is part of the final peak height for each position. When the noise is subtracted from the signal the mean stutter ratios are 0.070 ± 0.069 and 0.070 ± 0.013 for the low- and moderate-template samples, respectively. Figure 9 demonstrates the effects of noise when the starting template, T_0, is greater than 0. This plot shows the stutter ratios obtained for moderate (i.e., 0.25 ng; *Sim* 6) and low-template samples (i.e., 0.0078 ng; *Sim* 4) with and without the noise component removed. Stutter ratios for low-copy samples are substantially affected by the noise component, which can be as large and even exceed the signal generated by the stutter or allele fragment. In contrast, samples containing ample copy numbers are largely unaffected by the noise component since it is negligible compared to these peak heights. Despite the effects of noise on stutter ratios, the large variance of stutter ratio associated with low-template samples demonstrates that large stutter ratios are still expected for low-template samples and are not the result of noise effects alone.

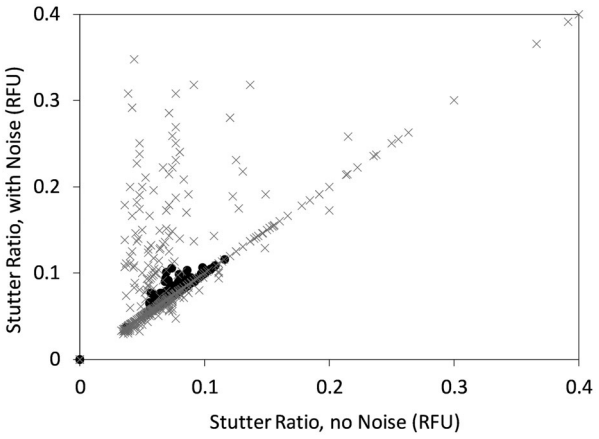

Figure 9. Stutter ratio with noise versus stutter ratio with noise component removed for (x) μ_{DNA} = 0.0078 and (•) μ_{DNA} = 0.25 ng/μL samples amplified using the parameters described in Table 1; *Sim* 4 and 6.

4 Discussion

We describe an in silico dynamic model of the full-DNA process from quantification to signal generation. For any analytical bioassay, the ultimate performance benchmarks are accuracy and reliability within the established dynamic range. To establish the sensitivity and dynamic range of any assay low-copy number validation standards may be artificially derived in the laboratory by serial dilution. A plethora of studies have indicated that this technique, though common, may need careful evaluation since volume transfer errors may propagate throughout the series [54, 55]; the implications being that the mass of the DNA is never known and approximations become prone to error as the sample is diluted. This study shows that even in cases where there is no pipette bias or variation, artificially generating low-template samples by employment of a dilution series strategy will lead to small, but real, differences in the numbers of alleles that survive the pre-PCR process. Additionally, the second study shows that moderate laboratory modifications that include small increases in injection time and cycle number are sufficient and result in signal to noise ratios large enough to confidently detect all signal—even signal from one copy of DNA if the PCR is uncompromised by external factors such as inhibitors, damage, or degradation. From a forensic processing perspective, this implies that a single optimized PCR and post-PCR laboratory protocol, such as the 29-cycle 20-s injection model here, will detect signal from even the smallest copy number and that the current technology has a potential LOD of one copy. Thus, once optimized post-PCR modifications have been implemented in the laboratory, improvements during pre-PCR sampling can be evaluated in order to enhance the number of copies that survive the pre-PCR process. Such improvements may include utilizing extraction strategies that decrease the volume of the extract such that a larger portion of the extract is processed through to PCR. Last, we highlight

the impact noise has on the ability to infer stutter ratios for samples in the single-cell regime and show that stutter ratio calculations are significantly perturbed by noise. Modeling of the relative stutter ratios by [32] indicated that the relative intensity of the stutter peaks increases with cycle number. As a result, these authors recommend an increase in injection time or voltage over an increase in cycle numbers, since an increase in cycle numbers would lead to more pronounced stutter peaks. As this work shows, increasing the sensitivity of the capillary system by increasing time or voltage is a viable option; however, stutter peaks from low-template samples or minor contributors are unlikely to reach RFU levels that are negligibly affected by noise without modification to the cycle number.

4.1 Conclusion

We developed a full-mechanistic mathematical model of the forensic laboratory process, creating a publically available implementation in the Stella environment. We utilized this simulation tool to synthesize D8S1179 EPGs in order to explore the impact of various laboratory conditions on the signal within the low-template regime. Low-template signal was also compared to signal generated from samples containing sufficient quantities of DNA. The model is capable of simulating synthetic EPGs at all template levels and is capable of delineating effects of noise, stutter, and allele peak heights on the total signal. The change in PCR efficiency with copy number, $E(N_c)$, and the CE sensitivity, α, were determined by a data-driven evaluation of the qPCR curve and CE RFU traces, respectively. We find good agreement between simulated and empirical data, which suggests the PCR efficiency and CE sensitivity were well characterized. For two of the simulation sets, *Sim* 4 and 5, there is sufficient signal to noise, suggesting that good separation between EPG signal obtained from one copy of DNA and noise is possible with only modest changes to laboratory protocols, such as increasing the injection time, or adding one additional cycle to the PCR. This also indicates that to be reasonably certain that all allele-based signal is detected, the commonly applied AT of 50 RFU coupled with the manufacturer's recommended protocol of $N_{PCR} =$ 28 or 29 and a 5-s/3 kV injection would require optimization. Further, stutter ratios obtained from low-template samples are not similar to ratios obtained from moderate-copy number samples and produce many stutter ratios that are greater than typical stutter thresholds generated using samples containing ample copy numbers. We determine that the large stutter ratios at the low-template region are, in many cases, a consequence of the additive noise interfering significantly with signal.

The authors thank Kevin Hallock, Kevin (Kip) Thomas, Kayleigh Rowan, and Peter Bergethon for helpful discussions. This project was partially supported by NIJ2014-DN-BX-K026 awarded by the National Institute of Justice, Office of Justice Programs, U.S. Department of Justice. The opinions, findings, and conclusions or recommendations expressed in this publication are those of the author(s) and do not reflect those of the Department of Justice.

The authors have declared no conflict of interest.

5 References

[1] Mullis, K., Faloona, F., Scharf, S., Saiki, R., Horn, G., Erlich, H., *Methods Enzymol.* 1986, *155*, 335–350.

[2] Gill, P., Curran, J., Elliot, K., *Nucleic Acids Res.* 2005, *33*, 632–643.

[3] Puch-Solis, R., Rodgers, L., Mazumbder, A., Pope, S., Evett, I., Curran, J., Balding, D., *Forensic Sci. Int. Genet.* 2013, *7*, 555–563.

[4] Cowell, R. G., Lauritzen, S. L., Mortera, J., *Forensic Sci. Int.* 2007, *166*, 28–34.

[5] Butler, J. M., *Forensic DNA Typing: Biology, Technology, and Genetics of STR Markers*, Elsevier, Burlington, MA, 2005.

[6] Bregu, J., Conklin, D., Coronado, E., Terrill, M., Cotton, R. W., Grgicak, C. M., *J. Forensic Sci.* 2012, *58*, 120–129.

[7] Buckleton, J. S., Curran, J. M., Gill, P., *Forensic Sci. Int. Genet.* 2007, *1*, 20–28.

[8] Biedermann, A., Bozza, S., Konis, K., Taroni, F., *Forensic Sci. Int. Genet.* 2012, *6*, 689–696.

[9] Paoletti, D. R., Krane, D. E., Raymer, D. L., Doom, T. E., *IEEE/ACM Trans. Comput. Biol. Bioinform.* 2012, *9*, 113–122.

[10] Benschop, C. C. G., Haned, H., Jeurissen, L., Gill, P. D., Sijen, T., *Forensic Sci. Int. Genet.* 2015, *19*, 92–99.

[11] Gilder, J., Doom, T., Inman, K., Krane, D., *J. Forensic Sci.* 2007, *52*, 97–101.

[12] Timken, M., Klein, S. B., Buoncristiani, M. R., *Forensic Sci. Int. Genet.* 2014, *11*, 195–204.

[13] Bieber, F. R., Buckleton, J. S., Budowle, B., Butler, J. M., Coble, M. D., *BMC Genet.* 2016, *17*, 125.

[14] Sanders, C., Sanchez, N., Ballantyne, J., Peterson, D. A., *J. Forensic Sci.* 2006, *51*, 748–757.

[15] Elliot, K., Hill, D., Lambert, C., Burroughes, T., Gill, P., *Forensic Sci. Int.* 2003, *137*, 28–36.

[16] Western, A., Nagel, J., Benschop, C., Weiler, N., Jong, B. D., Sijen, T., *J. Forensic Sci.* 2009, *54*, 591–598.

[17] Hedell, R., Dufva, C., Ansell, R., Mostad, P., Hedman, J., *Forensic Sci. Int. Genet.* 2015, *14*, 61–75.

[18] Smith, P., Ballantyne, J., *J. Forensic Sci.* 2007, *52*, 820–829.

[19] Rakay, C. A., Bregu, J., Grgicak, C. M., *Forensic Sci. Int. Genet.* 2012, *6*, 723–728.

[20] Walsh, P. S., Fildes, N. J., Reynolds, R., *Nucl. Acids Res.* 1996, *24*, 2807–2812.

[21] Gill, P., Gusmao, L., Haned, H., Mayr, W. R., Morling, N., Parson, W., Prieto, L., Prinz, M., Schneider, H., Schneider, P. M., Weir, B. S., *Forensic Sci. Int. Genet.* 2012, *6*, 679–688.

[22] Schneider, P. M., Fimmers, R., Keil, W., Molsberger, G., Patzelt, D., Pflug, W., Rothamel, T., Schmitter, H., Schneider, H., Brinkmann, B., *Int. J. Legal Med.* 2009, *123*, 1–5.

[23] Perlin, M. W., Szabady, B., *J. Forensic Sci.* 2001, *46*, 1372–1378.

[24] Taylor, D., Bright, J.-A., Buckleton, J., *Forensic Sci. Int. Genet.* 2013, *7*, 516–528.

[25] Cowell, R. G., Lauritzen, S. L., Mortera, J., *Forensic Sci. Int. Genet.* 2011, *5*, 202–209.

[26] Bright, J. A., Buckleton, J. S., Taylor, D., Fernando, M., Curran, J. M., *Electrophoresis* 2014, *35*, 3152–3157.

[27] Bright, J.-A., Taylor, D., Curran, J. M., Buckleton, J. S., *Forensic Sci. Int. Genet.* 2013, *7*, 296–304.

[28] Brookes, C., Bright, J.-A., Harbison, S., Buckleton, J., *Forensic Sci. Int. Genet.* 2012, *6*, 58–63.

[29] Gibb, A. J., Huell, A. L., Simmons, M. C., Brown, R. M., *Sci. Justice* 2009, *49*, 24–31.

[30] Life Technologies Corporation, *AmpFlSTR(R) Identifiler(R) Plus PCR Amplification Kit User's Manual*, Applied Biosystems 2006.

[31] Cowell, R. G., *Forensic Sci. Int. Genet.* 2009, *3*, 193–199.

[32] Weusten, J., Herbergs, J., *Forensic Sci. Int. Genet.* 2012, *6*, 17–25.

[33] Horsman, K. M., Hickey, J. A., Cotton, R. W., Landers, J. P., Maddox, L. O., *J. Forensic Sci.* 2006, *2006*, 758–765.

[34] Shewale, J. G., Schneida, E., Wilson, J., Walker, J., Batzer, M., Sinha, S. K., *J. Forensic Sci.* 2007, *52*, 364–370.

[35] Swango, K. L., Hudlow, W. R., Timken, M. D., Buoncristiani, M. R., *Forensic Sci. Int.* 2007, *170*, 35–45.

[36] DePamphilis, M. L., Bell, S. D., *Genome Duplication: Concepts, Mechanisms, Evolution and Disease*, Garland Science, London 2011.

[37] Kimmel, M., Axelrod, D., *Branching Processes in Biology*, Springer-Verlag, New York 2015.

[38] Wang, D., Chang, C.-W., Lagace, R. E., Calandro, L., Hennessy, L. K., *J. Forensic Sci.* 2012, *57*, 453–465.

[39] Monich, U. J., Duffy, K., Medard, M., Cadambe, V., Alfonse, L. E., Grgicak, C., *Forensic Sci. Int. Genet.* 2015, *19*, 107–122.

[40] Qiagen, *QIAamp(R) DNA Investigator Handbook*, Venlo 2010.

[41] BioRad Laboratories, *Chelex 100 and Chelex 20 Chelating Ion Exchange Resin*, Hercules, CA.

[42] Gevertz, J. L., Dunn, S. M., Roth, C. M., *Biotechnol. Bioeng.* 2005, *92*, 346–355.

[43] Stolovitzky, G., Cecchi, G., *Proc. Natl. Acad. Sci. USA* 1996, *93*, 12947–12952.

[44] Whitney, S. E., Sudhir, A., Nelson, R. M., Viljoen, H. J., *Comput. Biol. Chem.* 2004, *28*, 195–209.

[45] Lalam, N., *J. Theoret. Biol.* 2006, *242*, 947–953.

[46] Lalam, N., Jacob, C., Jagers, P., *Adv. Appl. Probab.* 2004, *36*, 602–615.

[47] Grgicak, C. M., Urban, Z. M., Cotton, R. W., *J. Forensic Sci.* 2010, *55*, 1331–1339.

[48] Life Technologies Corporation, *Quantifiler(R) Duo DNA Quantification Kit User Guide*, Foster City, CA, 2008.

[49] Rutledge, R. G., Stewart, D., *Plos One* 2010, *5*, 1–10.

[50] Tvedebrink, T., Eriksen, P. S., Mogensen, H. S., Morling, N., *Forensic Sci. Int. Genet.* 2009, *3*, 222–226.

[51] Kelly, H., Bright, J.-A., Curran, J. M., Buckleton, J., *Forensic Sci. Int. Genetics* 2012, *6*, 729–734.

[52] Gilder, J. R., Inman, K., Shields, W., Krane, D. E., *Int. J. Legal Med.* 2011, *125*, 87–94.

[53] Taylor, D., Bright, J.-A., McGoven, C., Hefford, C., Kalafut, T., Buckleton, J., *Forensic Sci. Int. Genet.* 2016, *20*, 6–19.

[54] Racine-Poon, A., Weihs, C., Smith, A. F. M., *Biometrics* 1991, *47*, 1235–1246.

[55] Higgins, K. M., Davidian, M., Chew, G., Burge, H., *Biometrics* 1998, *54*, 19–32.

